Journal of Materials Processing Technology. **231** pp. 288-300 (2016).
http://dx.doi.org/10.1016/j.jmatprotec.2015.12.011

Performance of Nickel and Bulk Metallic Glass as Tool Inserts for the Microinjection Molding of Polymeric Microfluidic Devices

Nan Zhang, Amit P. Srivastava, David J. Browne, Michael D. Gilchrist*

School of Mechanical and Materials Engineering, University College Dublin, Ireland
*Correspondence to: michael.gilchrist@ucd.ie

KEYWORDS
Feature replication; Tool performance; Electroforming; Thermoplastic forming

Abstract

Electroformed nickel and bulk metallic glasses (BMGs) can be designed to incorporate features with length scales ranging from millimeters to nanometers. This, combined with their good mechanical properties relative to other materials, makes them competitive candidates for manufacturing multi-scale molds to produce high volumes of polymeric microfluidics components and other micro/nano devices. Despite this attractiveness, BMGs are newly developed engineering materials and their capabilities as a mold material have not been evaluated. This paper compares the performance of nickel tools made by an electroforming process and BMG tools made by a thermoplastic forming process, specifically with regard to typical microfluidics patterns and features. Ni shows excellent capabilities for good feature replication. BMG thermoplastic forming is highly dependent on the choice of alloy composition, which restricts the achievable feature size and aspect ratio. Compared to Ni, BMG has hardness values that are close to those of stainless steel and shows the superior mechanical strength that is required for mass production applications. However, oxidation in BMG tool manufacturing process affects the tool surface finish significantly and reduces the tool's corrosion resistance. Future development of BMG tools include preventing the formation of oxidation layers or developing BMGs with an anti-oxidation composition, and further reducing their overall cost and widening its processing window parameters. Despite these challenges, however, BMGs are shown to combine excellent mechanical properties and capabilities for multi-scale forming; this makes them significantly more attractive than relatively soft Ni tools.

1. Introduction

Molded polymer microfluidic devices contain channels, the dimensions of which span hundreds of microns to hundreds of nanometers. Machining such small features is a challenge for manufacturing tooling technology. An ideal high performance tool should be strong and durable, capable of being manufactured to have features of particular size and aspect ratio, should maintain good de-molding capability with a reasonable draft angle, have an achievable appropriate surface finish and a good cost/performance ratio, and should retain its original geometry for at least 10^4 molding cycles without significant wear. Conventional mold construction uses tool steels, such as P20, which can last for 200,000-500,000 molding cycles with good tool maintenance. Stainless steel can be machined to have high aspect ratios and a user-defined draft angle using various micro-manufacturing technologies, such as micromilling, micro-EDM and laser micromachining. However, the micromilled trench

features cannot be smaller than 50μm, with a geometric tolerance of ±10μm, which is limited by the 50μm diameter of the smallest micromilling tools. Tool wear, when machining hard materials, influences the achievable accuracy, roughness, and generation of burrs (Uriarte et al., 2006). Micro-die EDM (electrical discharge machining) sinking has the problem of uneven wear of micro and macro features on the electrode. Micro-EDM milling has the challenge of compensating for electrode wear. When using laser micromachining, it is difficult to find an optimal process to achieve good quality outputs (Teixidor et al., 2013).

Among all of the various manufacturing technologies, electroformed nickel and bulk metallic glass are capable of integrating length scales ranging from millimeters to nanometers. Nickel electroforming is a metal deposition process whereby a nickel anode is dissolved into an electrolyte and thence deposits onto a conductive cathode upon applying a voltage, as shown schematically in Figure 1. The deposit on to the cathode is finally separated from an inverted substrate to form a single part. Electroforming itself is an established "atom-by-atom" technique, which can create a nearly perfect copy of the master geometry at virtually all scales. Ni tools have been used in injection compression molding to manufacture DVD and Blu-Ray Disks for mass production of low aspect ratio (<1) nanofeatures that range in size from 400nm to 150nm. It is the most widely used process for fabricating tools for injection molding of polymeric microfluidic devices.

Bulk metallic glass can be patterned at the nanometer scale either by using thermoplastic forming (Schroers, 2010) or Focused Ion Beam machining (Zhang et al., 2012a; Zhang et al., 2012b). In the thermoplastic forming process, BMG is heated into the supercooled liquid region (SCLR) above the glass transition temperature of the material and below its crystallization temperature, where it is easily deformed into a master mold and then cooled down, as shown in Figure 2. Metallic glasses in their supercooled liquid region are metastable and these materials tend to crystallize. However, the crystallization kinetics of glass-forming alloys are sluggish, which provides an opportunity to carry out thermoplastic forming without crystallization (David et al., 2009). BMG molds created by thermoplastic forming have been used for embossing of polymer microfluidics (Browne et al., 2013). Henann et al., (2009) thermoformed a commercial BMG, Vitreloy-1 ($Zr_{41.2}$ $Ti_{13.8}$ $Be_{22.5}$ $Cu_{12.5}$ Ni_{10}), with inverted channel features of height 43.5μm and width 55μm. The thermoplastic forming process was simulated based on their numerical modeling and the optimal process parameters were found to be 450°C with a holding pressure of 40MPa and a holding time of 2min. BMG was found to successfully reproduce features of a Si master and was used as a tool for embossing COC and PMMA. He et al., (2012) also used Zr based BMG ($Zr_{35}Ti_{30}Be_{26.75}Cu_{8.25}$) to thermoplastically form inverted microchannels 50μm wide and 100μm deep with a spacing of 200μm. Patterns were well replicated without any voids or material crystallization. The inverted patterns were successfully imprinted onto PMMA substrates. Our previous work has used BMG as a tool insert for micro/nano injection molding, where the smallest feature that was reproduced is 100nm (Zhang et al., 2012a).

Although Ni and BMG are comparable in achieving similarly sized features, the actual size of features that can be achieved using these two materials, and their respective mechanical properties, physical properties, tool life and associated costs are different. In our previous work (Zhang et al., 2015a), we have broadly discussed the performance of various tool materials, including stainless steel, Ni and BMG, but the tool features were not the same for each material tested. In the present work, we will focus on the replication of microfluidic patterns, including inverted channels and micro separation arrays and the testing of honeycomb structures and the evaluation of tool performance (cost, mechanical properties, surface finish, tool life) using large-area BMG and Ni tools based on microinjection molding using various plastic materials. Insights and key challenges regarding the development of mass production tools for polymeric microfluidic devices will also be discussed.

2. Experiments

2.1 Manufacturing processes for Ni and BMG tool inserts

2.1.1 Ni tool inserts

Standard UV-LIGA, and DRIE processes were used to transfer relatively high aspect ratio features onto a Si master, as shown in Figure 3. A Ni layer of approximately 300μm thickness was electrochemically deposited onto the substrate in a ready-to-use nickel bath under a well-defined recipe. Afterwards, the Si substrate was totally removed by wet etching with potassium hydroxide (KOH) at 82.8°C. CNC milling was then used to dice the Ni wafer into the dimensions of the mold insert and the uneven back surface was polished using SiC polishing paper. The finished Ni insert is shown in Figure 4 (b).

2.1.2 BMG tool insert

Large area BMG with a composition of $Zr_{44}Cu_{40}Al_8Ag_8$ was cast using an in-house tilt-casting technique following alloying and arc melting in an argon atmosphere. The Cu-Zr-Al-Ag system was chosen, because of its good glass forming ability, lack of toxic or prohibitively expensive elements, and reasonably high glass transition and service temperatures, enabling use for molding a variety of polymers (Browne et al., 2013). The amorphous nature of the BMG was confirmed using X-ray diffraction. Thermal characterization of BMG was carried out using differential scanning calorimetry (Netzsch DSC 200F3). Constant heating rate experiments were performed at 10 K/min and isothermal experiments were performed at various temperatures between 457°C and 480°C to generate the time-temperature transformation diagram (Figure 5 (a)). Viscosity was measured using Dynamic Mechanical Analysis (DMA) – Netzsch 242 Artemis – at 1 Hz with a heating rate of 0.2 K/min (Figure 5 (b)). The BMG materials were then machined and polished to achieve a surface roughness of less than 10nm. Microfluidic features were patterned on a Si wafer using standard lithography and deep reactive ion-etching (DRIE) techniques (Figure 3 (b)). The polished BMG and Si wafer were then heated to 472°C (745 K), above the BMG's glass transition temperature (710 K). Hot embossing was performed using a custom built apparatus attached to a Hounsfield uniaxial testing machine with a compression force of 25kN, which was held for 2min. The selection of these process conditions was based on optimization from previous trials using the same composition of BMG. The Si master was then dissolved in a KOH bath to expose the inverted BMG features. Finally, the BMG insert was machined using the EDM process in order to fit into injection mold.

2.2 Microfluidic chip design

The microfluidic chip that we designed contains two parallel inverted channels of width 800μm and height 50μm, as shown in Figure 6. Hexagonal pillar arrays were arranged on the center of the chip for testing purposes. The hexagons finally form honeycomb structures on the plastic parts. The diameters of the hexagonal pillars are 60 (group J), 45 (group I), 30 (group L) and 15μm (group K), respectively, and the spacing between individual patterns is 20, 15, 10 and 5μm, respectively. Two groups of heart-shaped patterns and wavy rectangular patterns were designed to mimic vascular systems and were used to study the behavior of sickle cells when flowing though blood vessels. Regarding pattern transfer, the hexagonal patterns were evaluated qualitatively. The heart-shaped patterns were compared using SEM images.

2.3 Feature mesurement and tool performance evaluation

A Veeco optical profilometer was used to measure surface roughness and feature height. Vickers hardness tests were performed to evaluate tool mechanical performance. A 5kg load was applied using a standard Vickers indenter in order to calculate the hardness of the tools. In order to test tool performance, all of the BMG and Ni inserts were evaluated in terms of the number of injection molding cycles. 600 molding cycles were carried out using each insert in a laboratory environment. Four different plastic materials were used: COC 8007 L10 (Cyclic Olefin Copolymer), PMMA VS-UVT (Poly(methyl methacrylate)), PP (Polypropylene) and Pebax 7233 (Poly (ether-block amide)). COC and PMMA are both transparent materials and have wide applications in polymer microfluidics. PP is a generic plastic material and Pebax is a medical grade elastomer. For the first 200 cycles, COC and PP were used as molding material. Then, after every 200 molding cycles, plastic materials were changed using either BMG or Ni inserts. Overall 600 molding cycles were carried out for each insert. Table 1 shows the injection

nozzle temperature and mold temperature, which represent the maximum and the minimum temperatures of thermal cycling of tool insert during the molding process.

3. Results and discussion

3.1 Feature replication

Figure 7 compares the replication of hexagonal patterns from a Si master using the thermoplastic forming and electroforming processes for BMG and Ni, respectively. It is obvious that the electroformed Ni has much better dimensional and geometric definition than the thermoplastically formed BMG. Regarding the BMG tool, groups I and K exhibit a clear surface on both the hexagonal patterns and the large ridges between the patterns. However, groups J and L show many surface fragments on top of the hexagonal patterns and on the large ridges. Such fragments were from a surface oxidation layer that formed during thermoplastic forming in an air atmosphere. This oxidation layer was also found on the inverted microfluidic channel, negative heart-shaped cavities and all of the surfaces of the tool (Figure 8 (a) and (b)), as indicated by the color change from a bright shiny finish after mechanical polishing to a dark matt surface with lots of surface impurities, (c.f. Figure 4 (a)). Some of the oxidation layer could be peeled off easily by hand but some still remained on the tool surface and the heart-shaped cavities (Figure 8 (c), (d)), where the oxidation layer was as thick as ~3.5μm.

Oxidation is common for most BMGs in the thermoplastic forming process, particularly when heated into the super cooled liquid region in air (Ze and Jan, 2015). Zr-based BMGs, such as Zr–Cu–Ni–Al, Zr–Ti–Cu–Ni–Be, etc., contain Zr, Al, Ti and Be, which are highly reactive to oxygen (Liu and Chan, 2005). It was also reported that in the filling of a nanometer size mold, this rigid oxide layer must be broken in order to allow BMG liquid flow into the pores, which limits the resolution to which Zr-based BMGs can be thermoplastically formed to no smaller than 1μm (Ze and Jan, 2015). Obviously, a thick oxidation layer would afford only a low degree of replication of small details and would influence feature integrity and accuracy.

While BMG can be thermoplastically formed to fabricate large-area microfluidic insert, there are some key practical issues that need to be considered. The first is the degree of parallelism between the two compression platens, which are used to sandwich the BMG and Si master together. For small-area samples, such as 6mm×6mm, Si is pressed directly into the BMG without any damage. However, for microfluidic inserts that are as large as 27.5mm×27.5mm, any tiny distortion of a compression platen easily cause the Si master to break. This actually happened in the present work: the crack was reproduced on the tool, as shown in Figure 9. In addition, the dimensions and distribution of features can lead to a non-uniform pressure distribution, which may also cause the Si master to crack or fracture. Moreover, any non-uniform contact also induces non-uniform surface oxidation. This is evidenced in the present work, where patterns K and I have a much clearer appearance than patterns J and L. This implies that the left side of the inserts (patterns I and K; Figure 4 (a)) has more intimate contact with the Si master than the right hand side. Uniform contact contributes to the prevention of surface oxidation when thermoplastic forming is carried out in an air atmosphere. It should be noted that, although this alloy was chosen for suitability as a tooling material (Zhang et al., 2015a), it is not resistant to oxidation in its SCLR. This is not a limitation of BMGs *per se*, and other more oxidation resistant BMG compositions exist but they may be prohibitively expensive or thermally unstable for the current molding applications.

The heights of the replicated patterns are listed in Table 2. The designed height of all patterns is 50μm. The heart-shaped cavity arrays have the minimum aspect ratio (height/width) ~ 0.64. BMG gives slightly better height accuracy (~48.8μm) than Ni (~48.5μm). However, the spacing between the heart-shaped arrays is not well replicated and has height ~15.3μm: this is due to an increased flow resistance and aspect ratio (2.5), as evident in Figure 8 (a). If the hexagonal patterns are considered, Ni exhibits much better replication than BMG (Figure 7). Feature replication using either Ni or BMG is dependent upon on the aspect ratio: smaller aspect ratios give better replication.

Ni inserts fabricated by the electroforming process are highly dependent on the precision of their corresponding masters. During Deep Reactive Ion Etching, the silicon etching rate decreases as the aspect ratio increases, because of ion flux loss at the bottom of the etched

structure (Lai et al., 2006). This phenomenon is referred to as "aspect ratio dependent etching" of the Bosch process. Electroforming can create a nearly perfect copy of the master geometry at virtually all scales. In the present work, the heights of the hexagonal patterns are 48.6, 46.0, 43.3 and 40.5μm, respectively, with the maximum relative dimensional error being 19%.

3.2 Tool performance

In this section, PP, COC, PMMA and Pebax were used to test Ni and BMG tools, since material-mold interaction (adhesion, wetting etc.) influences tool performance. Hardness, surface roughness and tool life were evaluated based on molding cycles. The tool cost and potential challenges regarding the development of mass production tools to manufacture polymeric microfluidics are also discussed.

3.2.1 Hardness

Changes in the hardness of the BMG and Ni inserts with increasing molding cycles are plotted in Figure 10. The Ni insert has a much lower hardness ~190HV5 than the BMG insert. Furthermore, there is a modest decrease in the hardness of the Ni insert with increasing molding cycles, from ~190HV5 to ~186HV5; such softening may be caused by thermally activate grain growth of Ni, which can be expected via the Hall-Petch relationship, where the yield stress of a polycrystalline material increases as the grain size decreases (Hansen, 2004).

The hardness indentations were carried out on both the clean oxide surface - underneath peeled off oxidation fragments, and on the surface where the oxidation layer remains present. The clean surface has a hardness of ~520HV5, while the oxidation surface has a higher hardness, 588HV5, because of the thick oxidation layer. The hardness increases initially and then remains essentially constant; this may be because the surface was cleaned by molten polymer during the first 200 cycles. The hardening may also be due to a thermal relaxation process which alters the atomic spacing in the BMG (Murali and Ramamurty, 2005).

3.2.2 Surface roughness

Figure 11 shows the average surface roughness of the Ni and BMG inserts. The Ni has two distinct regions, which are directly replicated from the Si master with wafer surface not etched by the deep reactive etching process. The inverted channel on the Ni insert is replicated from the etched channel on the Si master and has a relatively large surface roughness, ~15nm. The Ni surface that was replicated directly from the raw surface of the Si master that had been polished by Chemical Mechanical Polishing has a lower roughness, ~4.5nm. The roughness does not vary significantly during 600 molding cycles.

BMG has a much higher average surface roughness than the Ni insert, and also has a large standard deviation, which is mainly because of surface oxidation and its non-uniform distribution around different areas, as discussed above in Section 3.1. It appears that the surface roughness firstly decreases and then increases with molding cycles, which is associated with the evolution of the oxidation layer. This will be explained below.

3.2.3 Tool life

The tool inserts were examined using SEM in order to evaluate any surface wear and changes to feature integrity with increasing injection molding cycles. Figure 12 shows the appearance of BMG insert with the heart-shaped cavity arrays and the hexagonal patterns over increasing numbers of molding cycles. As discussed already, surface oxidation covers all tool surfaces with oxide fragments before any molding. Some of the oxidation layer is removed after thermoplastic forming and some remains on the tool surfaces. After 200 molding cycles with PP and COC, the oxidation layers were mostly removed by the polymer melts and the tool surface became noticeably cleaner. This was more pronounced after molding with Pebax, when almost all of the oxidation was removed from the hexagonal patterns and the boundaries of these features became clearer. It was also observed that some surface pitting occurred on the remaining oxide layer. These pits became larger when molding with PMMA and Pebax after 600 molding cycles. Additionally, the oxidation layer on top of the features also cracked. As shown in Figure 13, the integrity of the features was impaired by these pitting defects being on

top of the hexagonal patterns. The pitting defects on both the hexagonal arrays and the large ridges became denser and larger with increasing numbers of molding cycles. Some of the large pits contained crystalline-like inclusions, which was very similar to the morphology of pits on BMG after polarization in an NaCl electrolyte at 150°C (Gebert et al., 2001). It had been reported elsewhere that the formation of a surface oxidation layer made the nucleation process easier and the associated substrate was subsequently either partially or fully crystallized when heated to the super cooled liquid region (Zhang et al., 2014). When the original clear oxidation surface was examined in that work, it had porous structures, as indicated by semi-spherical cavities: this may be because of a more rapid diffusion-controlled growth which led to thick, porous layers, as noted by Gebert et al., (2001).

While the adhesion between the molten polymer and the BMG mold tends to clean the surface of the mold, it also enhances corrosion at initiation sites that are caused by surface oxidation. Possible further oxidation may also occur with increasing molding cycles. Zr-based BMG has been shown to exhibit enhanced corrosion resistance in halide-free solutions over a wide pH range at room temperature, because of the strong passivation ability of the main alloy component, Zr (Gebert et al., 1999). Such a passive layer is only a few nanometers thick. At elevated temperatures, Zr-based BMG exhibits strong accelerated corrosion in air with denser and larger particles forming on the surface, which become enriched with copper and oxygen (Zhang et al., 2014). Moreover, it was found that plastically deformed features are more prone to oxidation than undeformed areas (Hu et al., 2011). Figure 14 shows the compositional distribution across the height of the features after 600 molding cycles. Not all of the elements exhibit a significant variation from the top to the bottom of a feature, which indicates that the selected BMG composition can resist oxidizing during molding processes. In the injection molding process, the mold temperature is maintained below the polymer melt temperature and plastic deflection temperature, i.e., ~20°C to ~230°C. In such a repeatable process, the thickness of the oxidation layer on the BMG tool would increase with diffusion of O anions. Oxidation induced local crystallization accelerates pitting corrosion of the BMG tool and limits its long-term applications. Therefore, a BMG composition that has an anti-oxidization capability is critical for mold tool applications. Some BMG compositions, such as those based on noble metals like platinum or palladium are more resistant to corrosion and have high thermoplastic formability (Kana et al., 2011; Zhang et al., 2015b). However, these are prohibitively expensive in most manufacturing operations, and are less thermally stable than the current BMG alloy in use in this work. Rapid screening of BMG compositions is now possible via high throughput and parallel testing in combinatorial alloy development (Ding et al., 2014). It is also worthwhile noting that, since BMG materials are relatively brittle, care must be taken to avoid striking or dropping them or otherwise subjecting them to impacts, for example, when changing a mold or tool insert. Our particular experience has shown that, while the BMG was broken with cracks (Figure 13 (c)) due to unexpected operation during an insert change, the material remained amorphous, as seen by the XRD scans of Figure 15.

The electroformed Ni tool exhibits two failure modes when used in injection molding, namely, local surface fractures and pitting defects. In the first few cycles, Ni fragments adhere to polymer moldings and peel from the Ni substrate, as shown in Figure 16 (a) and (b). This behavior reduces after around 10 cycles, possibly because of rapid healing and repair. Such fracture is related to molding materials and processing. For example, we observed large broken fragments from the Ni surface in our previous work (Zhang et al., 2015a), which were directly related to surface adhesion from injection molding COC8007 for 130 cycles, especially when high temperature and high pressure conditions existed in the molding process, and demolding occurred close to material deflection temperature (Figures 16 (c)). However, in this present test, for the first 400 cycles, the Ni tool did not exhibit large surface fracture, when PP and PMMA were used as molding materials. The main reason for this was that the demolding temperature and injection pressure were much lower and adhesion between the Ni insert and polymer melts is not particularly strong during cooling and demolding. When processing Pebax for 400-600 cycles, on the other hand, Pebax adheres more strongly than the other polymers, even when the mold temperature is at ambient temperature, where peeling off a layer of Ni was observed from the Ni insert (Figures 16 (d)). Pitting corrosion is very common for Ni tools. It is known that

pits initiate at some chemical or physical heterogeneity of the surface, such as inclusions, second phase particles, solute-segregated grain boundaries, flaws and sites of mechanical damage or dislocations (Kolotyrkin, 1963). The process by which pits form is influenced by many environmental and material parameters, such as electropotential, alloy composition, electrolyte concentration, and temperature (Frankel, 1998). As far as the authors are aware, most corrosion research has been carried out in aqueous environments and there is little published literature on the pitting behavior of tool inserts exposed to molten polymer in the injection molding process. Regarding electroformed Ni tools, corrosion resistance has been found to be influenced by microstructure (grain size, surface morphology) and related electroforming parameters, such as current density, pH, plating bath composition, agitation and additives (Zamanzad-Ghavidel et al., 2009). For micro/nano molding, although Ni inserts have been used for ~10,000 cycles in the CD and DVD industries, the associated pits and lands have been noted to be small and with low aspect ratios; coatings, such as diamond-like carbon, have been used on Ni molds when producing CDs and DVDs (Ehmann et al., 2007). Additional coatings, such as TiN, are effective in protecting tools for ~20,000 cycles without significant wear (Tosello et al., 2012).

3.2.4 Cost analysis

Based on our experimental trials, the raw material cost for BMG ($Zr_{44}Cu_{40}Al_8Ag_8$) is ~€5.60×10^{-3}/mm^3. The material costs for Ni electroforming, including the Ni anode and the cost of the nickel sulfamate bath is ~€3.60×10^{-3}/mm^3, assuming that 40 runs can be achieved with one bath. Both BMG thermoplastic forming and Ni electroforming consume Si masters, which are assumed to cost the same, although conductive coatings need to be deposited on the Si master for electroforming. For electroforming, an SU8 master created from UV-lithography can be directly used as an electroforming master; this process chain could potentially decrease the associated material costs. The time required for BMG synthesis and thermoplastic forming (30×30×3mm) is estimated to be 2 days. Electroforming of one 4-in wafer to produce a 0.4mm thick shim takes about four days. In addition, the BMG thermoplastic forming process is completely green and causes no potential environmental pollution, unlike the Ni electroforming process.

3.3 Comparison of Ni and BMG tools

Here we summarize the benefits and drawbacks of BMG and Ni tooling in terms of feature replication, roughness, mechanical properties and tool performance. BMG thermoplastic forming is a mechanical thermo-deformation process and the quality of feature replication depends on the formability of the BMG former in the supercooled liquid region. Thermoplastic forming of BMG is governed by the Hagen–Poiseuille flow (Schroers, 2005),

$$P = \frac{16\eta}{t_{cryst}}\left(\frac{L}{d}\right)^2 + 4\frac{\gamma}{d} \quad (1)$$

where γ is the surface tension of the alloy melt and P is the pressure required to fill a liquid of viscosity η into a channel of thickness d and length L by the time for the material to reach crystallization t_{cryst}. The equation has been modified to take into account the capillary effect at small length scales that decides the filling of the supercooled metallic melt into the small sized features. From this equation, the required filling pressure increases with the aspect ratio (L/d). It is not surprising that a high aspect ratio gives less filling because of increasing flow resistance. An optimum processing window with low viscosity and long processing time is required. In practice for embossing, the operation time is selected from an operational point of view and shorter than material crystallization time. Thus, the viscosity is fixed from the TTT diagram for a certain composition. For microfluidic chips, the channel dimensions may be fixed. The only parameter that can be optimized is the applied pressure. The maximum applied pressure is limited by the fracture strength of the master for a particular strain rate. Si masters are very brittle and are easily fractured during embossing because of any non-uniform pressure distribution. Too much pressure leads to a high strain rate, which causes insufficient filling because of the inhomogeneous and non-Newtonian flow (Li et al., 2013). For the present work,

the smallest hexagonal cavity has a nominal width of 15μm and depth of 50μm. A pressure of ~8889MPa is required to fill BMG into such a small cavity, assuming that a reasonable operation time (time for the material to reach crystallization) of 120s and embossing temperature of 472°C (corresponding viscosity, η , is ~3000 MPa-s) are selected. This pressure exceeds the strength of the Si master and, consequently, cannot be achieved when using the current BMG composition. In addition, because of the non-slip flow boundary, the flow front of the BMG hexagon is parabolic and additional pressure and time are required to fully fill the cavity with dimensional and geometric accuracy. Electroforming is an electro-chemical stress-free deposition process. The achievable feature size is influenced by the feature's aspect ratio because of ion diffusion in the metallization and electroforming processes. In designing microfluidic devices, high aspect ratio features should be avoided in order to reduce the difficulties of filling in fabrication tools using BMG and to avoid causing possible damage to polymer features that need to be demolded from micro cavities. Overall, Ni has higher replication fidelity than BMG for tooling applications.

BMG is significantly harder than Ni. In theory, this should mean that BMG has greater longevity when used as a production tool. However, because of oxidation, pitting corrosion of the current BMG alloy is comparable to that of Ni after only several hundred molding cycles. Our previous work used a Focused Ion Beam milled BMG tool for injection molding of nano-patterns, and this was used successfully for ~20,000 cycles (Zhang et al., 2012b). Therefore, thermoplastic forming of BMG under inert and high vacuum environments should provide BMG tools that have far longer lifetimes than a Ni insert. BMG can be polished or otherwise prepared to have a very high surface finish, with a surface roughness as small as single nanometers. Again, surface oxidation could cause an increase of surface roughness if a proper vacuum or inert gas environment is not used. The roughness of a Ni tool depends on the Si master, and typically ranges from 4~18nm. However, surface fractures in the first ten to twenty cycles may introduce some toxic elements into the molded plastic chip. The use of BMG is limited to producing relatively small size parts, depending on glass-forming ability.
The discovery of new BMG composition that has a balanced combination of a large processing window, good oxidation resistance, high mechanical strength, long tool life, and good wear resistance for an acceptable price is critical for micro/nano tooling applications.

4. Conclusion

This work compares the performance of Ni and BMG tools for the production of polymer microfluidic components using the microinjection moulding process. Ni shows excellent capabilities for good feature replication, because of the low stresses associated with this atom-by-atom electrodeposition process. Regarding thermoplastic forming of BMG, the processing window (supercooled liquid region) for thermoplastic forming is highly dependent on the choice of alloy composition, which restricts the achievable feature size and aspect ratio. Compared to Ni, BMG has hardness values that are close to those of stainless steel and it has the superior mechanical strength that is required for mass production applications. Oxidation that occurs during thermoplastic forming is found to be a critical problem for BMG. It affects the tool surface significantly and reduces the tool's corrosion resistance. Oxidation of BMGs can be avoided by using either vacuum or inert gases during thermoplastic forming, or via selection of more noble compositions that are still compatible with forming an amorphous material.

BMGs combine excellent mechanical properties and capabilities for multi-scale forming; this makes them significantly more attractive than the relatively soft Ni tools. However, considerable challenges remain in scaling up the BMG thermoplastic forming process from a laboratory environment to a commercial production environment. Other challenges to using BMG as molding tools include preventing the formation of oxidation layers or developing BMGs with an anti-oxidation composition, and further reducing their overall cost and widening its processing window parameters.

Acknowledgements

The authors gratefully acknowledge financial support from Enterprise Ireland (Grant Nos. CFTD/07/314, CF/2012/2022 and CF/2012/2640B) and the European Regional Development Fund. The authors also thank Tyndall National Institute for access to their semiconductor fabrication facilities. The involvement of groups of UCD's MEEN40110 students in helping to test the tool inserts with the injection molding process is also acknowledged.

References

Browne, D.J., Stratton, D., Gilchrist, M.D., Byrne, C.J., 2013. Bulk metallic glass multiscale tooling for molding of polymers with micro to nano features: a review. Metall and Mat Trans A 44, 2021-2030.

David, L.H., Vikas, S., Hayden, K.T., Melinda, R.H., David, E.H., Lallit, A., 2009. Metallic glasses: viable tool materials for the production of surface microstructures in amorphous polymers by micro-hot-embossing. Journal of Micromechanics and Microengineering 19, 115030.

Ding, S., Liu, Y., Li, Y., Liu, Z., Sohn, S., Walker, F.J., Schroers, J., 2014. Combinatorial development of bulk metallic glasses. Nat Mater 13, 494-500.

Ehmann, K.F., Bourell, D., Culpepper, M.L., Hodgson, T.J., Kurfess, T.R., Madou, M., Rajurkar, K., DeVor, R., 2007. Micromanufacturing: International Research and Development. Springer Netherlands.

Frankel, G.S., 1998. Pitting corrosion of metals a review of the critical factors. Journal of the Electrochemical Society 145, 2186-2198.

Gebert, A., Buchholz, K., El-Aziz, A.M., Eckert, J., 2001. Hot water corrosion behaviour of Zr–Cu–Al–Ni bulk metallic glass. Materials Science and Engineering: A 316, 60-65.

Gebert, A., Buchholz, K., Leonhard, A., Mummert, K., Eckert, J., Schultz, L., 1999. Investigations on the electrochemical behaviour of Zr-based bulk metallic glasses. Materials Science and Engineering: A 267, 294-300.

Hansen, N., 2004. Hall–Petch relation and boundary strengthening. Scripta Materialia 51, 801-806.

He, J.J., Li, N., Tang, N., Wang, X.Y., Zhang, C., Liu, L., 2012. The precision replication of a microchannel mould by hot-embossing a Zr-based bulk metallic glass. Intermetallics 21, 50-55.

Henann, D.L., Srivastava, V., Taylor, H.K., Hale, M.R., Hardt, D.E., Anand, L., 2009. Metallic glasses: viable tool materials for the production of surface microstructures in amorphous polymers by micro-hot-embossing. Journal of Micromechanics and Microengineering 19, 115030.

Hu, Z., Li, L., Hu, Y., Xing, J., Wei, B., 2011. Oxidation features of plastic deformed Zr-based bulk metallic glass. Journal of Alloys and Compounds 509, Supplement 1, S69-S73.

Kana, T., Noriko, S., Nobuyuki, N., Akihisa, I., 2011. Fabrication and nano-imprintabilities of Zr-, Pd- and Cu-based glassy alloy thin films. Nanotechnology 22, 105302.

Kolotyrkin, J.M., 1963. Pitting corrosion of metals. Corrosion 19, 261t-268t.

Lai, S.L., Johnson, D., Westerman, R., 2006. Aspect ratio dependent etching lag reduction in deep silicon etch processes. Journal of Vacuum Science & Technology A 24, 1283-1288.

Li, N., Chen, Y., Jiang, M.Q., Li, D.J., He, J.J., Wu, Y., Liu, L., 2013. A thermoplastic forming map of a Zr-based bulk metallic glass. Acta Materialia 61, 1921-1931.

Liu, L., Chan, K.C., 2005. Oxidation of Zr 55 Cu 30 Al 10 Ni 5 bulk metallic glass in the glassy state and the supercooled liquid state. Appl. Phys. A 80, 1737-1744.

Murali, P., Ramamurty, U., 2005. Embrittlement of a bulk metallic glass due to sub-T g annealing. Acta Materialia 53, 1467-1478.

Schroers, J., 2005. The superplastic forming of bulk metallic glasses. JOM 57, 35-39.

Schroers, J., 2010. Processing of bulk metallic glass. Advanced Materials 22, 1566-1597.

Teixidor, D., Ferrer, I., Ciurana, J., Özel, T., 2013. Optimization of process parameters

for pulsed laser milling of micro-channels on AISI H13 tool steel. Robotics and Computer-Integrated Manufacturing 29, 209-218.
Tosello, G., Hansen, H.N., Gasparin, S., Albajez, J.A., Esmoris, J.I., 2012. Surface wear of TiN coated nickel tool during the injection moulding of polymer micro Fresnel lenses. CIRP Annals - Manufacturing Technology 61, 535-538.
Uriarte, L., Herrero, A., Ivanov, A., Oosterling, H., Staemmler, L., Tang, P.T., Allen, D., 2006. Comparison between microfabrication technologies for metal tooling. Proceedings of the institution of mechanical engineers, Part C: Journal of mechanical engineering science 220, 1665-1676.
Zamanzad-Ghavidel, M.R., Raeissi, K., Saatchi, A., 2009. The effect of surface morphology on pitting corrosion resistance of Ni nanocrystalline coatings. Materials Letters 63, 1807-1809.
Ze, L., Jan, S., 2015. General nanomoulding with bulk metallic glasses. Nanotechnology 26, 145301.
Zhang, M., Yao, D., Wang, X., Deng, L., 2014. Air oxidation of a Zr55Cu30Al10Ni5 bulk metallic glass at its super cooled liquid state. Corrosion Science 82, 410-419.
Zhang, N., Byrne, C.J., Browne, D.J., Gilchrist, M.D., 2012a. Towards nano-injection molding. Materials Today 15, 216-221.
Zhang, N., Chu, J.S., Byrne, C.J., Browne, D.J., Gilchrist, M.D., 2012b. Replication of micro/nano-scale features by micro injection molding with a bulk metallic glass mold insert. Journal of Micromechanics and Microengineering 22, 065019.
Zhang, N., Srivastava, A., Kirwan, B., Byrne, R., Fang, F., Browne, D.J., Gilchrist, M.D., 2015a. Manufacturing microstructured tool inserts for the production of polymeric microfluidic devices. Journal of Micromechanics and Microengineering, 22, 095005.
Zhang, X., Ma, J., Fang, G., Sun, B., Li, J., Li, Q., 2015b. Polymer micro molding with bulk metallic glass mold. Microsyst Technol 21, 1453-1457.

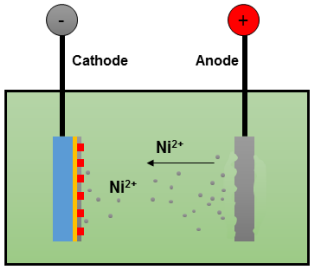

Figure 1. Nickel electroforming process to fabricate micropatterned tool.

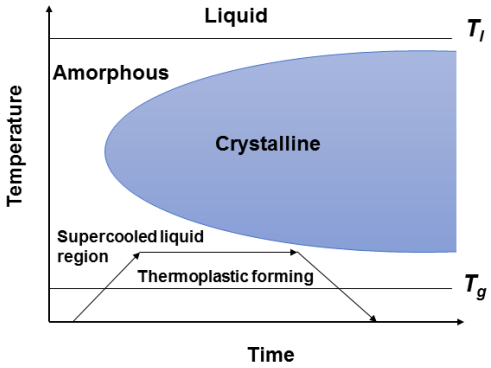

Figure 2. A schematic time–temperature-transformation (TTT) diagram for a typical BMG, where T_l is the liquidus temperature and T_g is the glass transition temperature.

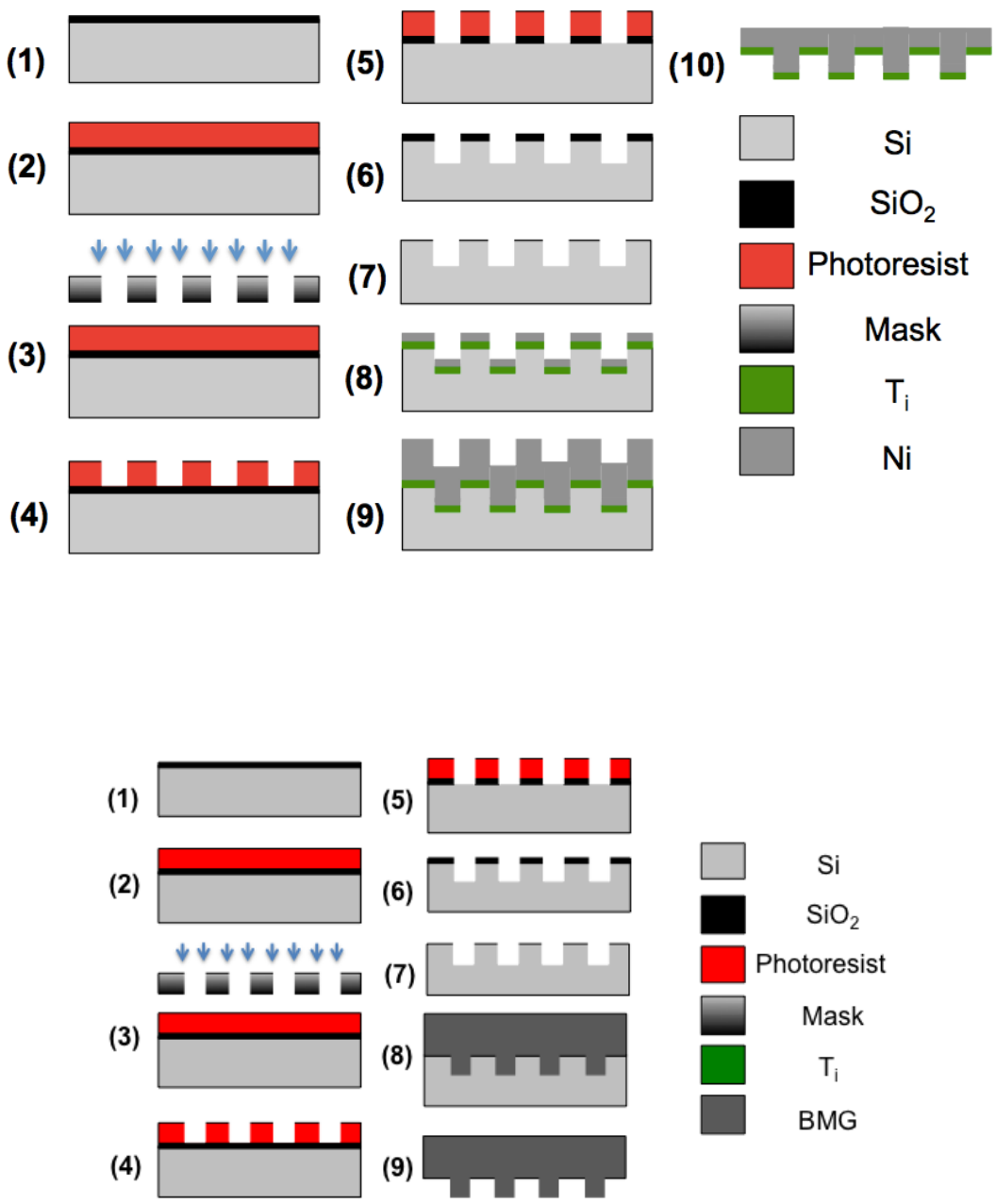

Figure 3. Process chains for manufacturing of Ni and BMG tool inserts: (a) UV-LIGA process: (1) Si oxidation, (2) Spin coating photoresist, (3) UV lithography, (4) Development, (5) etching SiO_2 and removing photoresist, (6) RIE etching of Si, (7) PVD Coating Ti and Ni, (8) electroplating, (9) Si dissolving, (10) Ni wafer dicing and polishing; (b) Thermoplastic forming process: (1)-(7) are the same as with the UV-LIGA process, (8) BMG thermoplastic forming into Si master, (9) Si dissolving in KOH solution.

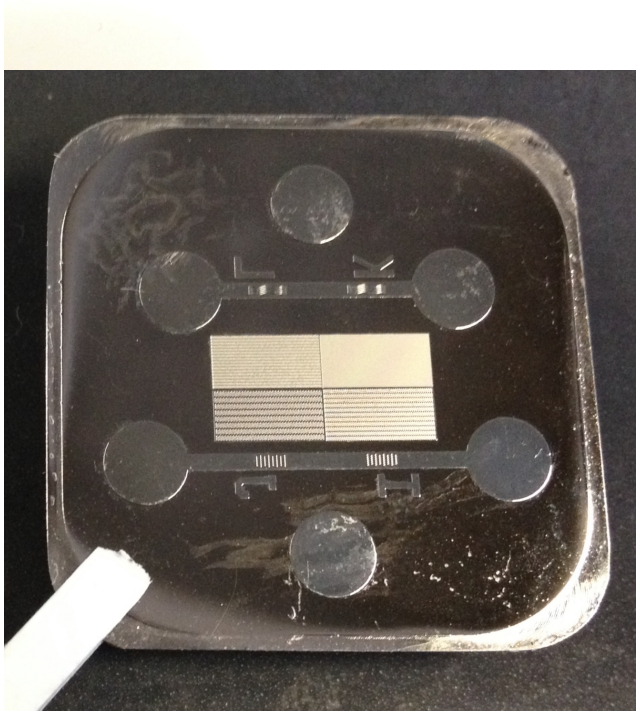

Figure 4. Thermoplastic formed metallic glass tool (a) and Ni tool (b) (27.5×27.5mm).

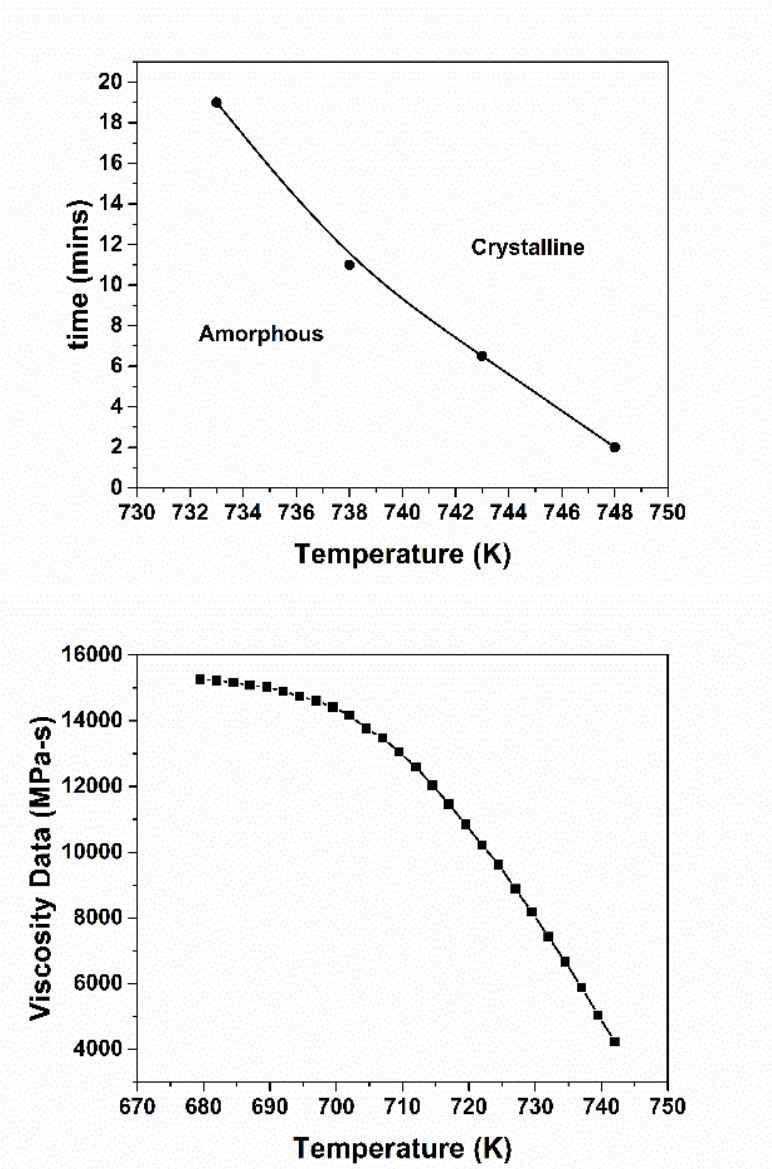

Figure 5. T-T-T curve showing transformation from glassy state to crystalline state in BMG (a) and viscosity measured using DMA at 1 Hz and heating rate of 0.2 K/min (b).

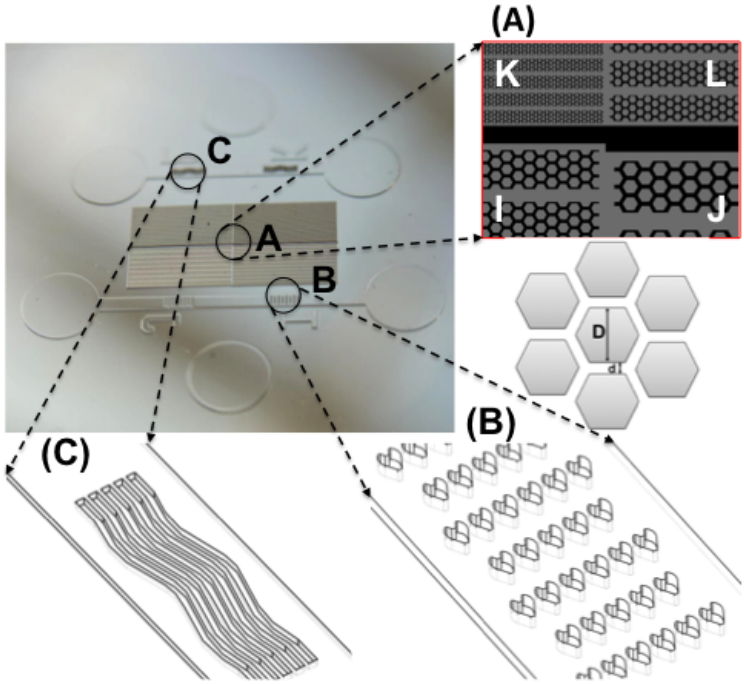

Figure 6. Designed microfluidic features (overall chip is 27.5mm×27.5mm).

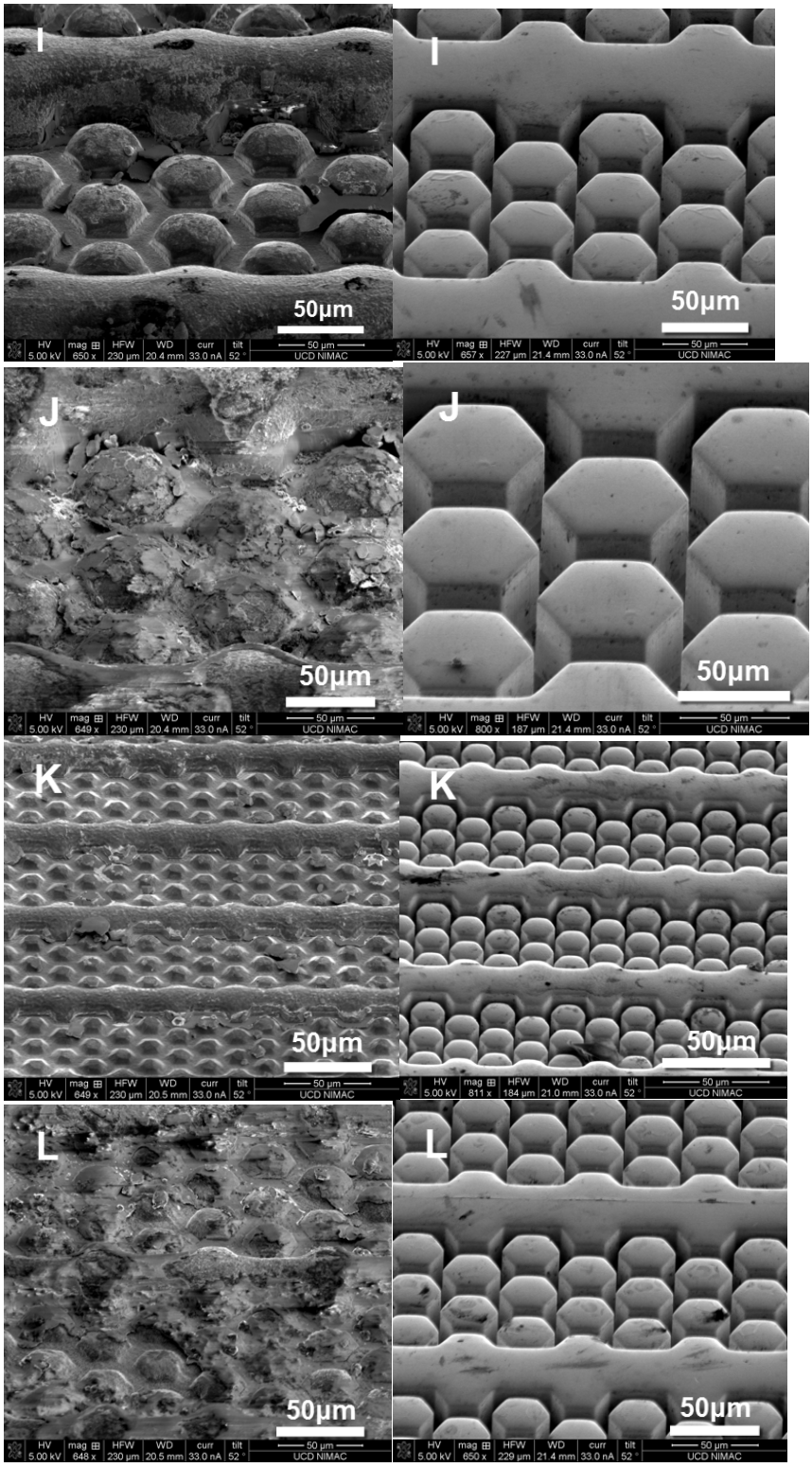

Figure 7. Comparision of the replication of hexagonal patterns using BMG thermoplastic forming (left) and Ni electroforming (right) with diameter of (a) 45µm (group I), (b) 60µm (group J), (c) 30µm (group K), (d) 15µm (group L).

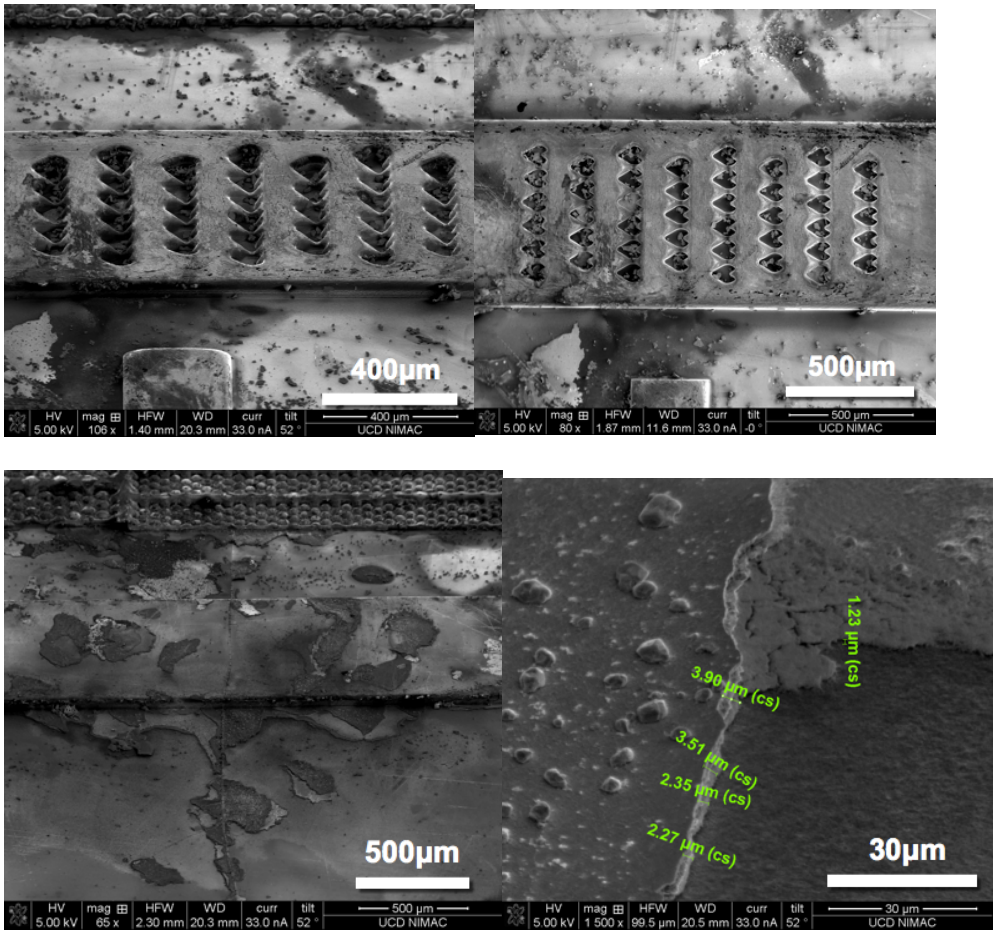

Figure 8. Replicated BMG patterns: (a) and (b) are heart-shaped cavities located on an 800µm wide inverted channel, (c) is inverted channel pattern and (d) shows the interface of the peeled off and remaining oxidation layers.

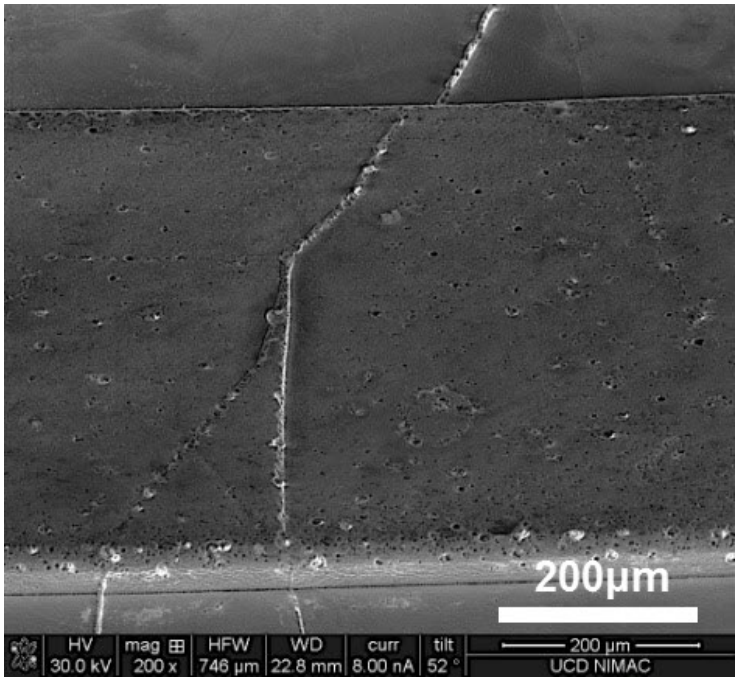

Figure 9. Protrusions formed by pressed BMG into cracks on the Si master.

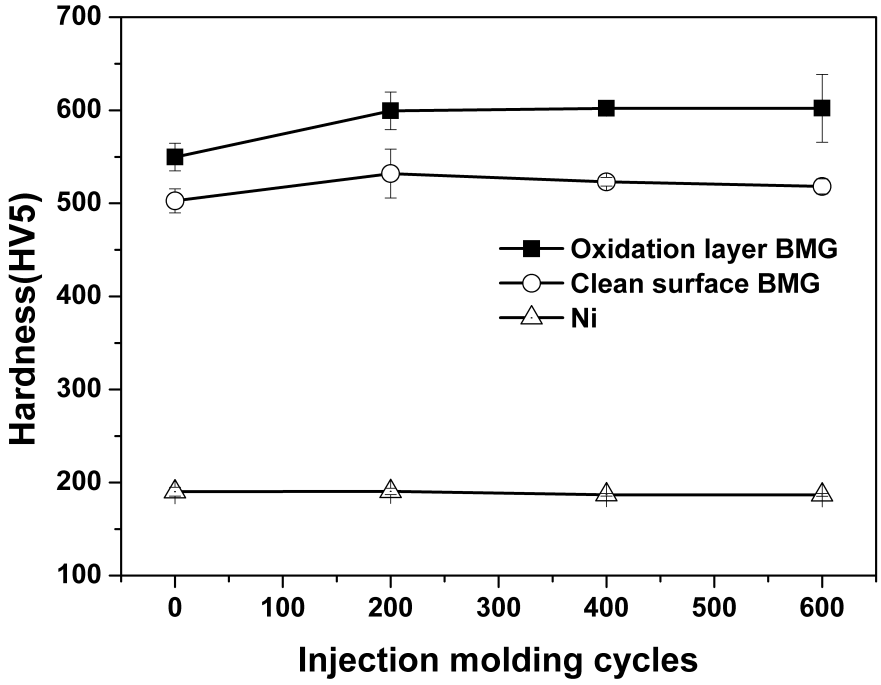

Figure 10. Hardness of BMG and Ni insert with increasing molding cycles.

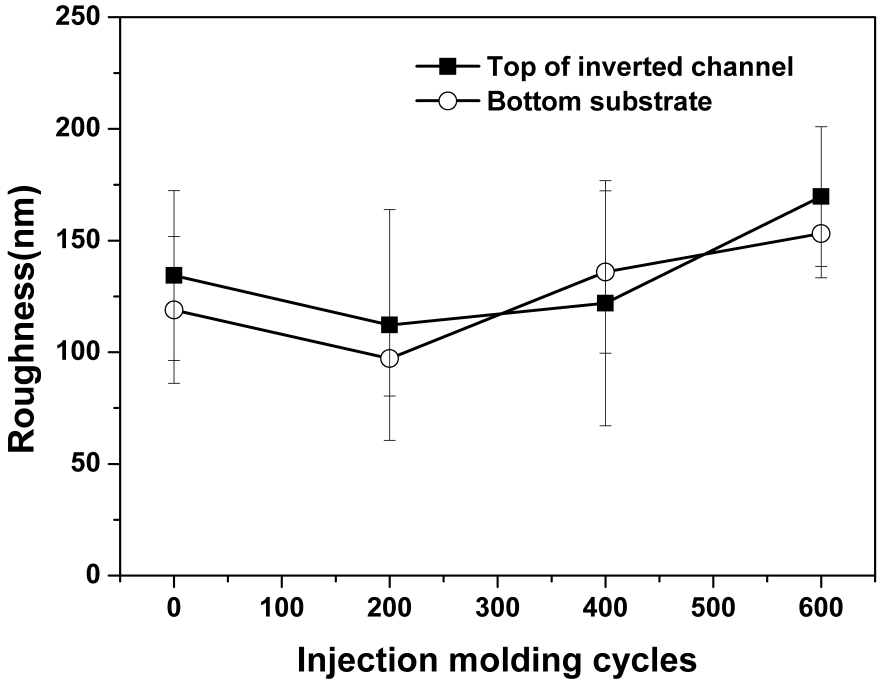

Figure 11. Roughness changes for the Ni (a) and BMG (b) inserts with increasing molding cycles.

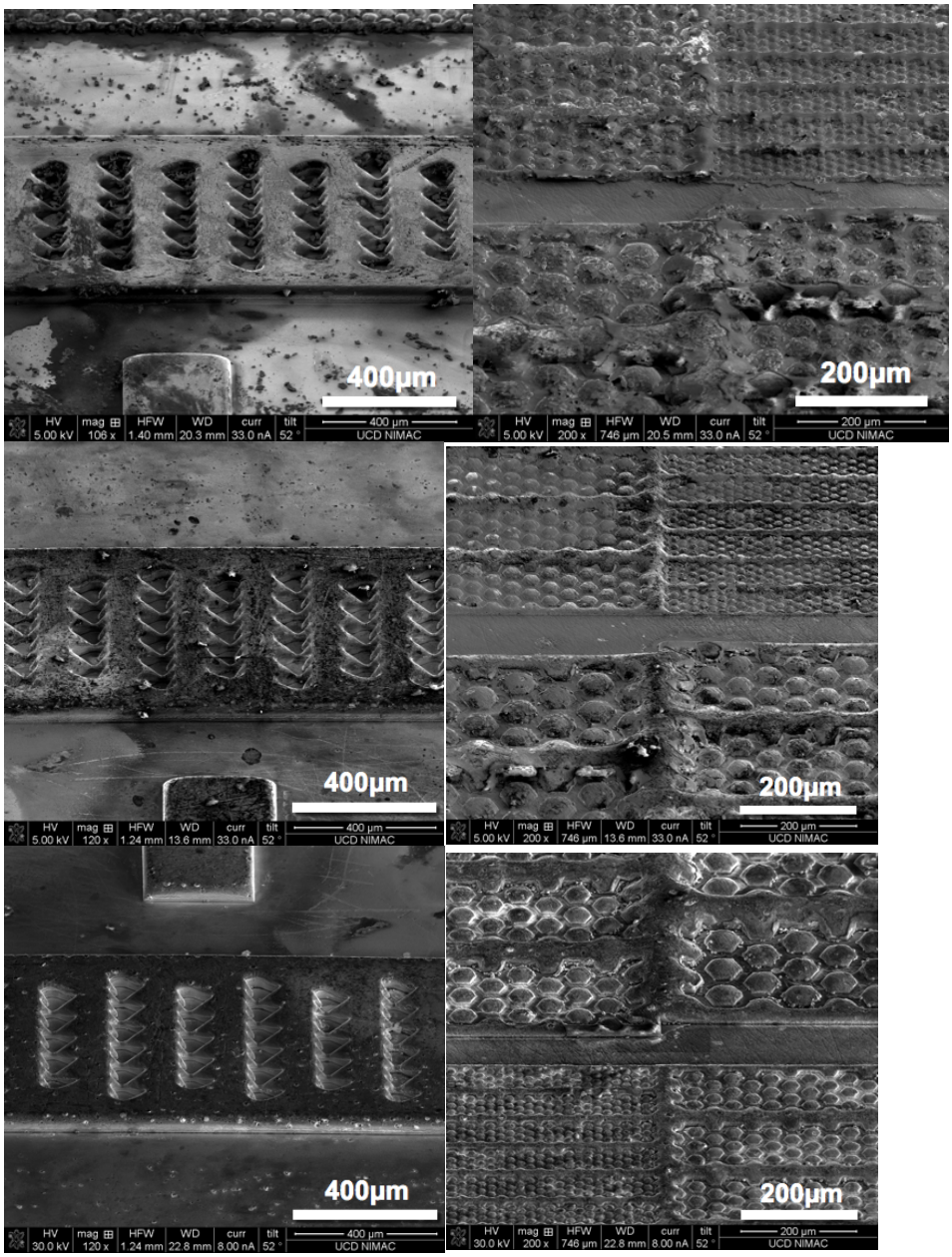

Figure 12. Changes of BMG tool surface conditions with molding cycles: (a) before use, (b) after 200 cycles, and (c) after 600 cycles.

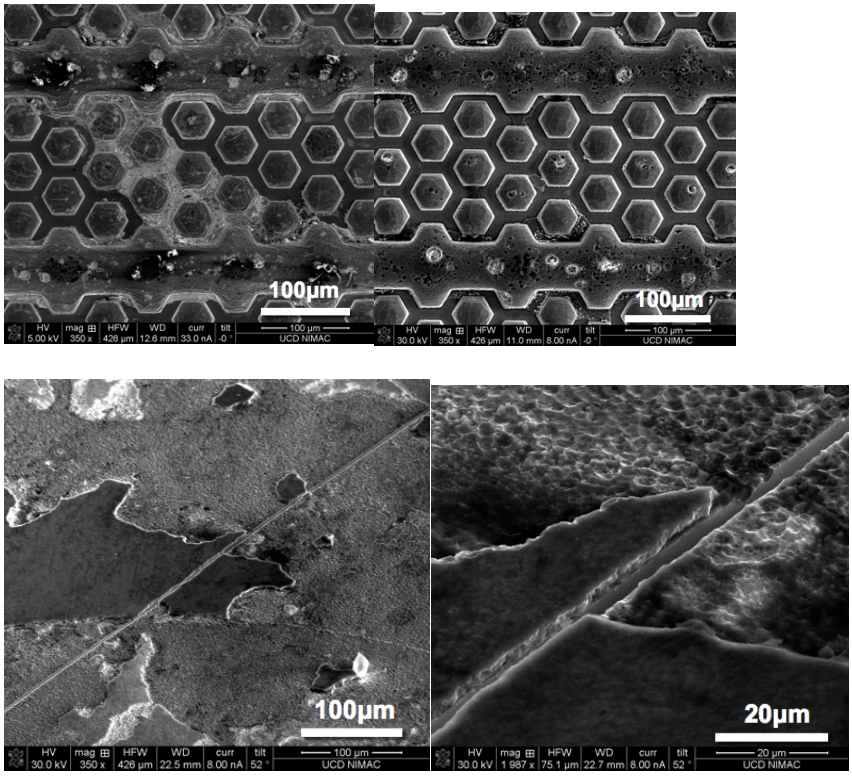

Figure 13. Evolution of surface pitting on BMG tool with molding cycles: (a) 200 cycles, (b) and (c) 600 cycles. It is noteworthy that cracks formed on the BMG tool as evident in (c); these were due to unexpected operation during an insert change, although the material remained amorphous.

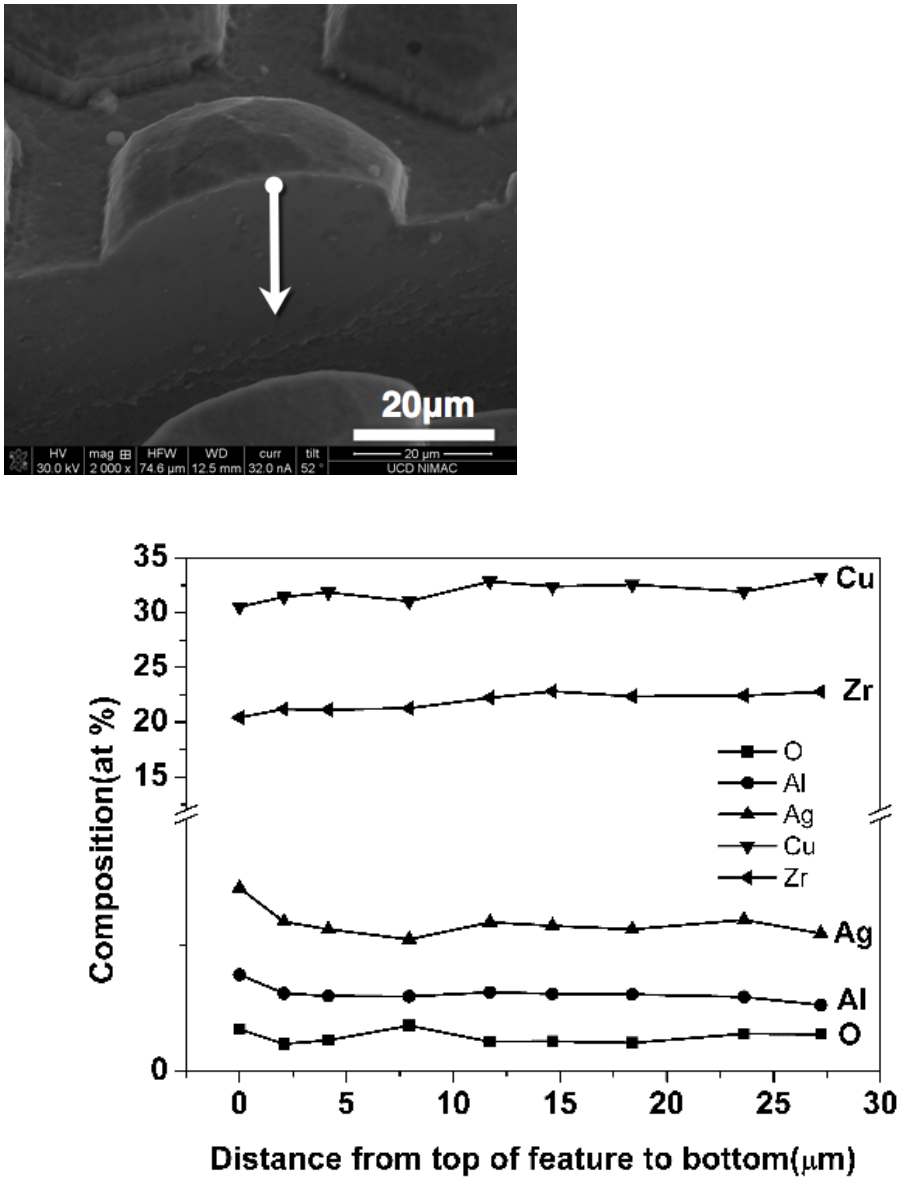

Figure 14. The compositional distribution across a 45µm hexgonal pattern from the top to the bottom of the feature: (a) feature; (b) compositional distribution.

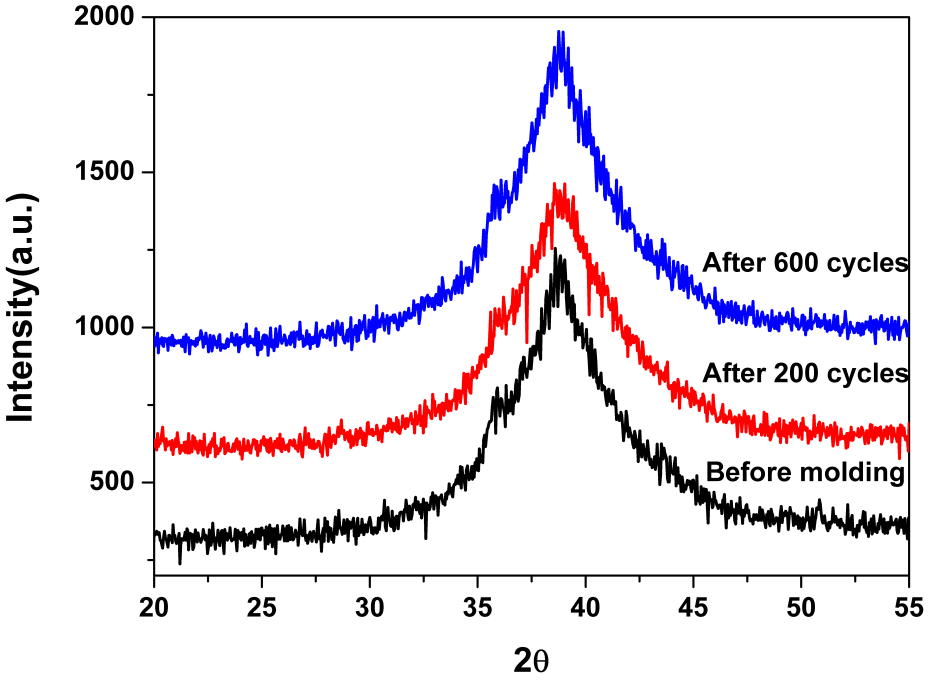

Figure 15. XRD scan of the top BMG tool insert before and after injection molding; clear absence of major cystalline peaks.

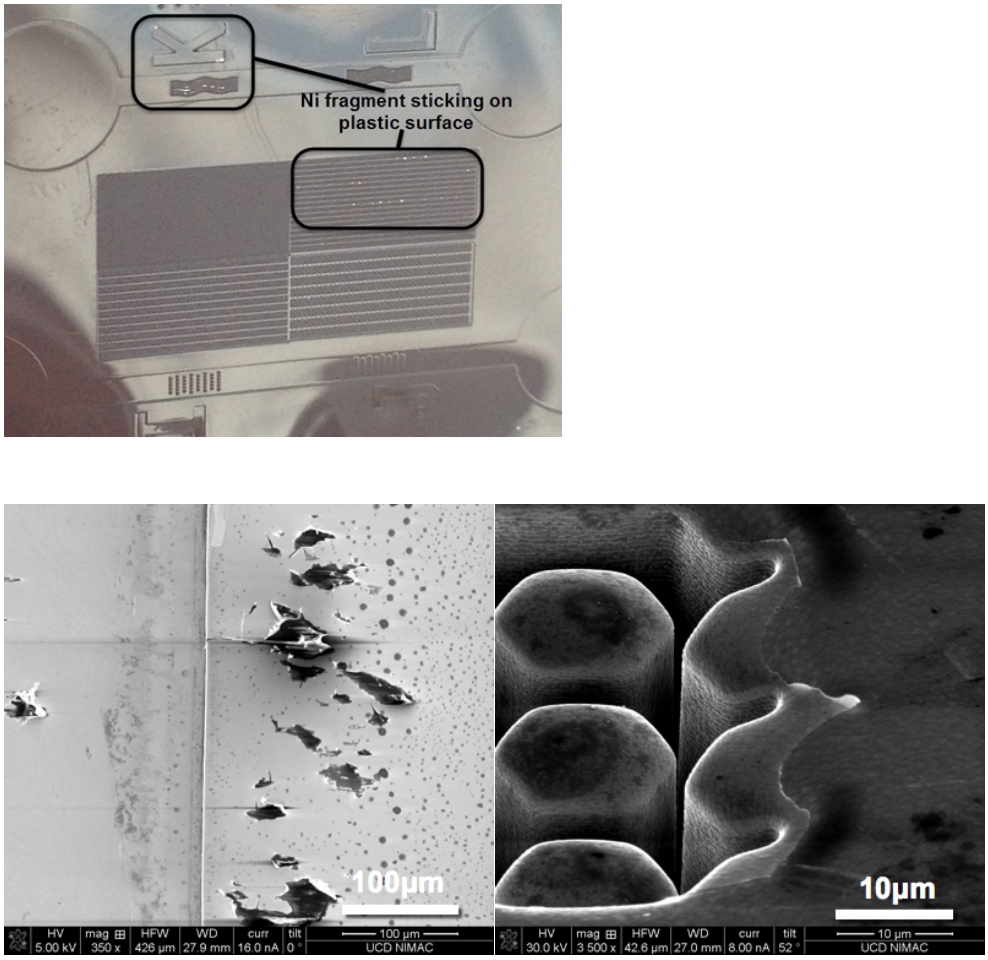

Figure 16. Failure of Ni tool with increasing molding cycles: Ni fragments stick to plastic surface features when molded with Polypropylene (a) and are visible under an optical microscope when enlarged (b); (c) Inverted channel feature shows surface cracks, pittings and inclusion after 130 molding cycles using COC (using another cassette mold in the reference work (Zhang et al., 2015a)); (d) peeling off of Ni surface layer after 600 molding cycles using PEBAX material (using same mold with BMG insert in the present work).

TABLES

Table 1. Processing temperature of injection molding tests using various polymer materials.

	COC	**PMMA**	**PP**	**Pebax**
Melt temperature	230 °C	220 °C	210 °C	210 °C
Mold temperature	60 °C	60 °C	60 °C	20 °C

Table 2. Replicated height of microfluidic patterns (μm) (c.f. Figure 6).

	Heart-shaped pattern	**Spacing between heart patterns**	**Hexagon pattern I**	**Hexagon pattern J**	**Hexagon pattern K**	**Hexagon pattern L**
BMG	48.8±0.56	15.3±0.42	16.1±0.73	19.01±0.54	2.9±0.36	4.7±0.28
Ni	48.5±0.07	48.4±0.08	46±0.10	48.6±0.72	40.5±0.13	43.3±0.91